

Dynamic modelling and analysis of the potential for waste heat recovery on Diesel engine driven applications with a cyclical operational profile

Francesco Baldi^a, Stephanie Lacour^b, Quintan Danel^c and Ulrik Larsen^d

^a *Department of Shipping and Marine Technology, Chalmers University of Technology, Gothenburg, Sweden. francesco.baldi@chalmers.se*

^b *Irstea-GPAN, Antony Cedex, France, stephanie.lacour@irstea.fr*

^c *Laboratoire de Chimie Moléculaire, Génie de Procédés Chimique et Energétiques (CMGPCE – EA21), Conservatoire national des arts et métiers, Paris, France. quintin.danel@outlook.fr*

^d *Department of Shipping and Marine Technology, Chalmers University of Technology, Gothenburg, 41 296 Sweden. ulrik.larsen@chalmers.se*

Abstract:

As the world faces the challenge of the need for decreasing the anthropogenic carbon footprint, the continuous economic growth puts additional stress on the need for increased energy systems efficiency. In this context, waste heat recovery is identified as one of the most viable solutions for reducing the fuel consumption of existing systems in transportation.

In this paper, we present an analysis of the potential of a waste heat recovery system applied to Diesel engine-driven systems where the operational cycle is dynamic but reducible to a limited number of operational modes. The analysis is applied to a case study for which this operational pattern is of particular relevance: a machine for sugar beet harvesting. The existence of periodical low-load periods forces to bypass the waste heat recovery turbine to avoid water condensation during the expansion. Hence, we propose the use of a thermal inertia to keep the required level of steam superheating during low-load periods.

The results of the study showed an improvement of 27% in the recoverable exergy of the flow at the heat exchanger cold outlet when the heat exchanger wall thickness was increased from 0.5 mm to 2.5 mm. The results also show that a limited amount of the overall heat exchange inertia contributes to such improvement

Keywords:

Waste heat recovery; Diesel engines; dynamic modelling; agricultural machines;

1. Introduction

Internal combustion engines (ICE) are by large the most employed prime mover technology for transportation, in particular on land and sea. Their wide diffusion, together with the expected increasing trend in fuel prices and the challenge of global warming, has led to widespread efforts aiming at reducing ICEs fuel consumption.

More than half of the energy input to an ICE is wasted to the environment in the form of hot exhaust gas or cooling water [1] and for this reason waste heat recovery systems (WHRS) are among the most studied solutions for improving ICEs energy efficiency [2].

Among the different technologies available for WHR applications to ICEs, the Rankine cycle is traditionally regarded as one of the most efficient and reliable solutions [2]; extensive work has been proposed in relation to the application of Rankine cycles in road transport (see, among others, [3–8]), as well as in the maritime sector [9–15].

Road and maritime applications normally differ markedly in terms of their operative conditions. WHRS design for application in international shipping focuses on steady-state conditions (and, often, on one individual operating point) due to typically stationary operations of such systems. On the other hand, road applications require focus on transient operations, which leads to the existence of extensive literature on WHR control systems [16,17]. Even in the latter case, however, although

observations from real operations are sometimes used to weight the selected operating points (see, for instance, [4]), the WHRS design still relies on steady state methods. Heating and cooling periods are sometimes considered [18] but this is mainly done in order to estimate the time of response rather than for optimising the heat recovery potential.

Non-road machinery, particularly agricultural machines, and inland shipping vessels constitute a significant share of respectively land- and sea-based transportation. These vehicles generally follow clearly identifiable operating cycles which are significantly dynamic but follow a determinate, repeatable pattern. In addition, compared to cars and trucks, these applications show higher engine load coefficient and exhaust temperatures [4,5,19,20]. Hence, being in between steady-state generator and heavy-transient road engines for both size and transient behaviour, heavy non-road engines (marine or agriculture) should have specifically designed heat recovery systems.

Several studies are dedicated to the dynamic performance of single-phase heat exchangers [22,23] as well as to two-phase ones [17,24,25]; however, the subject of the optimisation of the design of the WHRS evaporator based on dynamic cycle performance still remains unclear.

The aim of this paper is to study the dynamic behaviour the boiler heat exchanger of a WHRS, which is the dynamically most critical part of the system [16,21]. Focus is on analysing how different design parameters, of a tubular exchanger, influence the recovery potential, with particular focus on the role of the inertia of the heat exchanger wall.

2. Method

2.1 Activity monitoring

Three sugar beet harvesters are selected to participate in a campaign designed to cover the whole season of harvest. A tractor with a smaller engine was also equipped and monitored more than a year to get a whole cultural cycle. The choice of the vehicles was made so to be representative of the most commonly employed agricultural machines on the European market. The experiment campaign was conducted in between September 2011 and December 2012 for the harvesters and from November 2010 up to February 2012 for the tractor. Details about these agricultural machineries are given in the Table 1, while more information concerning the operations of gathering and processing the measured data is available in [26].

Table 1. Summary of the machines involved in the experimental campaign

Name	Moreau Lexis		Vervaeet Beet	Holmer	MF 6475
Year of experiment	2011	2012	2011	2012	2011
Number of operations	53	74	68	126	132
Record duration (hours)	104	214	257	788	330
Hours per operations	3.14	3.96	5.35	7.43	2.5
Engine type	PENTA		DAF	MAN	PERKINS
	TWD1240VE		MX13.375	D2876 LE	1106D-E66TA
Engine power (kW)	275	275	375	383	105

More information on the gathering and processing of measured data is available in [26].

2.2 Determination of the reference cycle

Four main operational conditions for the selected machines were identified:

- Transport (high speed)
- Harvesting (high speed and torque)
- Idling (zero torque)
- Transition (intermediate torque)

All measured points were categorised as above, and the distributions of engine operations in terms of speed and torque are represented in Figure 1:

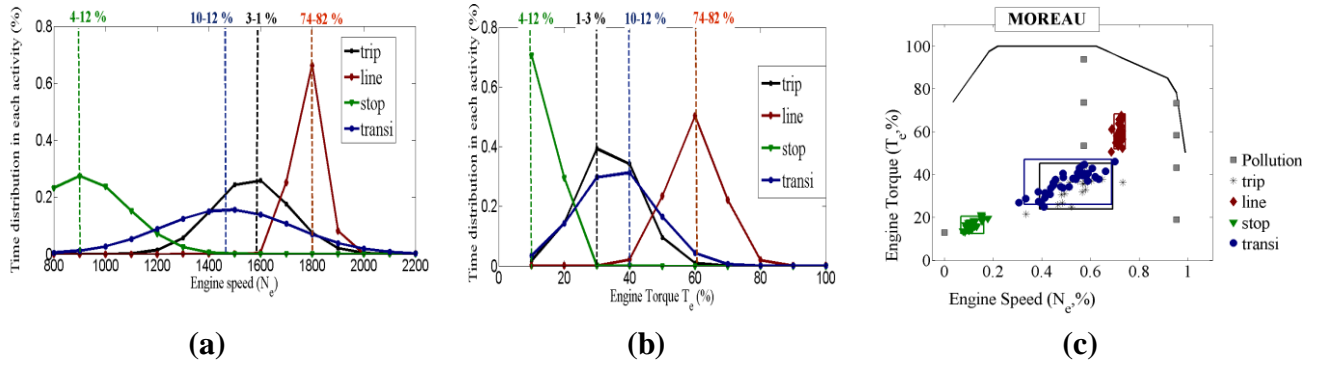


Fig. 1: Statistic distribution of the harvesting operations. (a) Engine speed; (b) engine torque; (c) speed versus torque

The analysis of the measured data suggests that the amount of time spent for transport is just 3% of the total and it corresponds to a very broad spectrum of engine speed and power. Such behaviour is also observed in the “transition” phase, up to 12% of the time, which corresponds to manoeuvres and to short distance transfers between fields.

The average duration of the harvesting phase was calculated to 7.5 hours, with little variation between different machines. This phase takes the largest share of machines operations and is carried out in a regular manner, in proximity of a fixed operational point which varies between different fields only to a limited degree. Operational breaks of the duration of 20-50 minutes are relatively common but unpredictable; finally, 4-12% of the time is spent idling, which generally happen for a duration of 208 seconds. Finally, transitions between one working line and the following one generally last 53 seconds.

The temperature and mass flow rate of the exhaust gas are measured on a dynamometer for different engine speeds and torques, see Fig. 2. The measurements show that, while the exhaust gas temperature is relatively high during the harvesting phase, it drops to lower levels during idling and manoeuvring. A similar behaviour can also be observed for the exhaust gas flow.

The cyclic operations of the studied machines during harvesting can be observed in Figure 3a. Since the harvesting part of the operations occupies the largest share of the time and occurs at high loads, this condition presents the largest potential for improvements in fuel consumption.

Starting from the conditions observed during measurement campaigns and represented in Figure 3a, a reference cycle was selected for the simulation of the dynamic behaviour of the evaporator. The simulated conditions in terms of inlet temperature and mass flow at the hot inlet are represented in Figure 3b, and include an initial warming-up period of 600 seconds, followed by three working cycles of 360 seconds each, composed of 300 seconds harvesting (with exhaust temperature and flow respectively of 623 K and 0.25 kg/s) and 60 seconds manoeuvring (523 K and 0.15 kg/s).

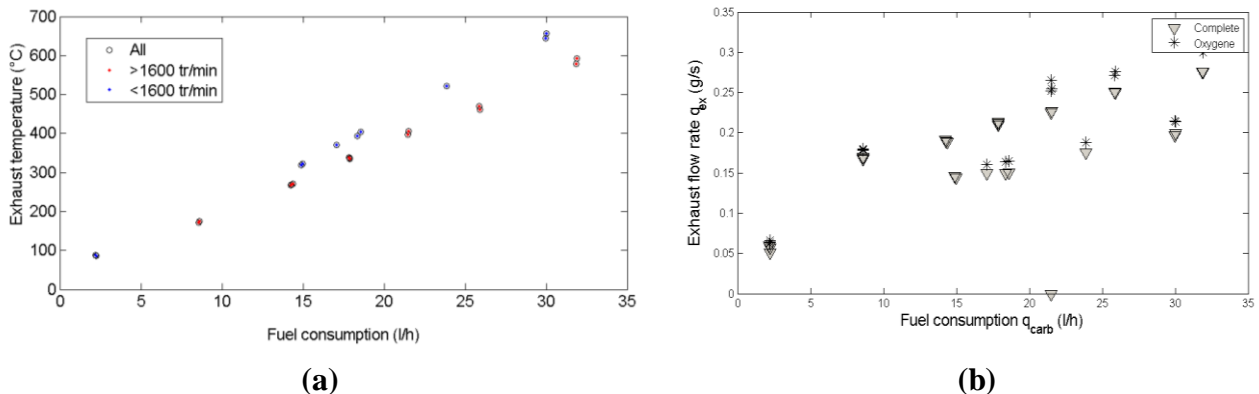


Fig. 2 - Exhaust temperature (a) and exhaust flow rate (b) according to fuel consumption measurements made on a bench test for steady-state conditions for the Perkins engine.

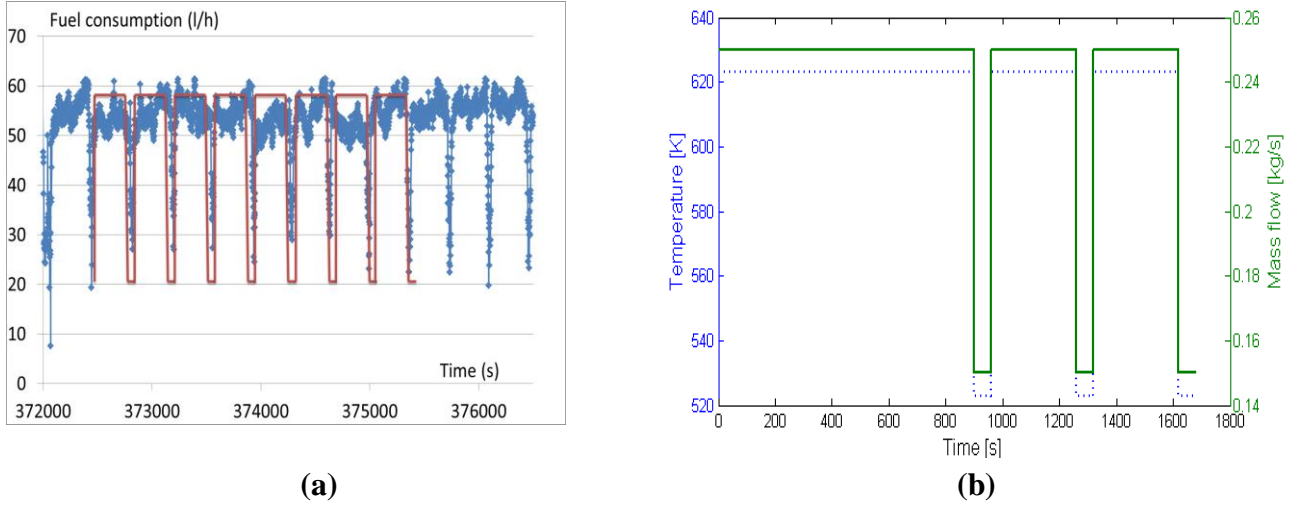


Fig. 3. Operational profile for the case under study. (a) Fuel consumption versus time, from measured data. (b) Exhaust gas temperature and mass flow rate employed in the simulations. The relationship between engine fuel consumption and exhaust gas temperature and mass flow rate are derived from measurements performed in controlled testing facilities.

3. Heat exchanger

3.1 Dynamic heat exchanger modelling

In order to model the dynamic performance of the heat exchanger, as previously described, a one-dimensional model, based on the principle of finite volumes, was set up. Although computationally more expensive, finite volume models are more numerically reliable in dynamic simulation [27]. A number of 40 equally sized volumes was selected as a good compromise between computational time and intensity of numerical instabilities. For each volume the following set of equations was solved at the metal of the inner pipe:

$$dQ_m (x_i, t_j) =$$

$$\left[\dot{Q}_{hm} + \dot{Q}_{cm} + \lambda_m A_m (T_m (x_{i+1}, t_j) - T_m (x_i, t_j)) + \lambda_m A_m (T_m (x_{i-1}, t_j) - T_m (x_i, t_j)) \right] dt, \quad (1)$$

$$\dot{Q}_{hm} (x_i, t_j) = h_{hm} A_{hm} [T_h (x_i, t_j) - T_m (x_i, t_j)], \quad (2)$$

$$\dot{Q}_{cm} (x_i, t_j) = h_{cm} A_{cm} [T_c (x_i, t_j) - T_m (x_i, t_j)], \quad (3)$$

Where λ_m represents the thickness of the heat exchanger wall, A_{hm} and A_{cm} the outer and inner surface of the wall respectively, A_m the heat exchange surface between the elements of the wall, and the subscripts h,c and m respectively represent the hot, cold fluid and the wall metal.

The heat transfer coefficients h_{cm} and h_{hm} are calculated as follows:

$$h_{hm} = \left(h_h^{-1} + \frac{\ln(r_{w,e} / r_{w,i})}{2\lambda_m} \right)^{-1}, \quad (4)$$

where the convective heat transfer coefficients h_h and h_c are estimated using correlations available from scientific literature. For the hot fluid and for the cold fluid in sub-cooled liquid and superheated vapour forms the Colburn correlation was used, which has the following form:

$$Nu = 0.023Re^{0.8} Pr^{(1/3)}$$

The two-phase heat exchange coefficient was calculated using the correlation based on fluid quality reported by [28] for convection boiling and hereafter reported:

$$h_{2ph}(x) = h_{l0} \left\{ (1-x)^{0.01} \left[(1-x)^{1.5} + 1.2x^{0.4} R^{0.37} \right]^{-2.2} + x^{0.01} \left[\frac{h_{l0}}{h_{g0}} \left(1 + 8(1-x)^{0.7} R^{0.67} \right) \right]^{-2} \right\}^{0.5}, \quad (5)$$

Where h_{l0} and h_{g0} represent the convective heat flow of the liquid and the gas phases, calculated using the Colburn correlation, x is the quality and R is the ratio of the density of the liquid over the gas phase. This correlation has the advantage of being continuous with quality. In order to reduce computational time, the coefficients of (6) are calculated once when the first boiling occurs, and then updated as a function of the mass flow on the hot side as proposed by Quoilin [27] and shown in (7):

$$h_{2ph} = h_{(2ph,nom)} \left(\frac{\dot{m}_h}{\dot{m}_{h,nom}} \right)^{0.5}, \quad (6)$$

The evolution of the temperatures in the heat exchanger over time is calculated according to a Eulerian approach; the properties at the instant $j+1$ are therefore calculated based on the heat exchange properties evaluated at the instant j . For the heat exchanger wall this reduces to (7):

$$T_m(x_i, t_{j+1}) = T_m(x_i, t_j) + dQ_m(x_i, t_j), \quad (7)$$

For the hot and cold fluid, the equation of mass and energy conservation (Equations 8 and 9) were solved simultaneously:

$$V_i \frac{d\rho}{dt} \Big|_{i,t} = \dot{m}_{i-1,t} - \dot{m}_{i,t}, \quad (8)$$

$$\frac{dU}{dt} \Big|_{i,t} = \dot{m}_{i-1,t} h_{i-1,t} - \dot{m}_{i,t} h_{i,t} + dQ_{i,t}, \quad (9)$$

By combining (8) and (9) the explicit form can be obtained:

$$\frac{\partial \rho}{\partial h} \Big|_{i,t}^{-1} \dot{m}_{i,t} + \left[\frac{\partial \rho}{\partial h} \Big|_{i,t}^{-1} - \left(\frac{h_{i-1,t} - h_{i,t}}{\rho_{i,t}} \right) \right] \dot{m}_{i-1,t} = \frac{\dot{Q}_{i,t}}{\rho_{i,t}}. \quad (10)$$

Equation (10) is only valid under the assumption of constant pressure. This assumption was used in order to save computational time and because in this study it was decided to have constant inlet pressure on both sides of the heat exchanger. Pressure losses and their influence of the thermal behaviour of the two fluids were hence neglected.

The presence of fast transients can lead of numerical instabilities and to the insurgence of back flows, particularly in relation to the sharp variation in the density of water in proximity of the liquid saturation line. In this case this was solved as suggested by Quoilin et al. [29] by smoothing the density function between saturated liquid and vapour with 0.1 quality. This solution, although physically incorrect, allows minimizing inaccuracies in energy and mass balance, while keeping low computational time and ensuring high numerical robustness [29].

Further assumptions were employed for the sake of reducing computational time:

- Uniform specific heat in the exhaust gas, calculated at the mean temperature in the exhaust of the previous time step.
- Ideal gas behaviour for water vapour. This assumption is justified given the low water/steam pressure employed in this study [30].
- Equal vapour heat exchange properties during evaporation and condensation. The heat exchange coefficient of the two-phase mix on the cold side of the exchanger was assumed to

only depend on the vapour quality as expressed in Equation (5), with no distinction between evaporation and condensation.

3.2 Heat exchanger design

For the case under study it was decided to use a simple concentric pipe design in order to reduce the complexity of the simulation. The heat exchanger is designed to have the hot fluid flowing in the outer pipe, while the cold fluid flows in four smaller inner pipes. This configuration is chosen in order to enhance the heat exchange surface while keeping a limited flow area on the cold side. The temperature of the hot fluid is considered to be uniform radially. A sketch of the heat exchanger cross section is provided in Figure 4.

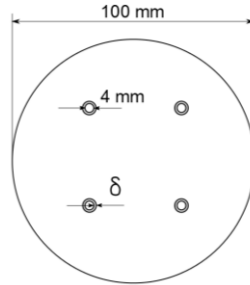


Fig. 4. Cross-section of the heat exchanger modelled in this study.

Table 2 summarises the geometric parameters of the heat exchanger in the reference case. These are chosen as a compromise between obtaining a reasonable degree of superheating at the steam outlet of the exchanger and reducing the physical size of the exchanger. Copper is chosen as material for the heat exchanger, and it is assumed that thermal properties (conductivity, specific heat capacity and density) are constant with temperature.

Table 2: Summary of the reference geometrical parameters of the heat exchanger

Property	Unit	Value
Length	m	40
Diameter hot side	mm	100
Diameter cold side (inner)	mm	4
Diameter cold side (outer)	mm	6
Number of pipes (cold side)	-	4

The influence of the thickness of the inner pipe in the tubular heat exchanger as a mean for increasing heat exchanger inertia was tested in this study. The integral of the exergy flow at the outlet of the exchanger on the cold side over a full manoeuvring and working cycle was used as a performance indicator. It was also assumed that if the quality of the cold fluid at the heat exchanger outlet dropped below one, the exergy flow available for recovery is equal to zero.

$$\dot{EX}_{rec} = \begin{cases} 0 & \text{if } h_{c,out} < h_{vsat} \\ \dot{m}_c [(h - h_0) - T_0 (s - s_0)] & \text{if } h_{c,out} \geq h_{vsat} \end{cases} \quad (11)$$

This corresponds to a hypothetical control system bypassing the recovery turbine in specified conditions of the cold fluid to prevent turbine damaging as a result of the formation of droplets in the final turbine stages.

3.3 Simulations

The model described in Sections 3.1 and 3.2 was used to simulate the behaviour of a tubular heat exchanger where the hot fluid is subject to variations in inlet flow and enthalpy.

The hot fluid is exhaust gas of a Diesel engine, with a molar composition of 67% nitrogen, 10% oxygen, 12% carbon dioxide and 11% water, and a pressure of 0.11 MPa. The cold fluid used in this study is water, at a pressure of 0.4 MPa and a mass flow of 0.015 kg/s; these values were chosen based on the requirement of having superheated steam at the heat exchanger cold outlet with a sufficient degree of superheating. Water inlet conditions are assumed to be constant.

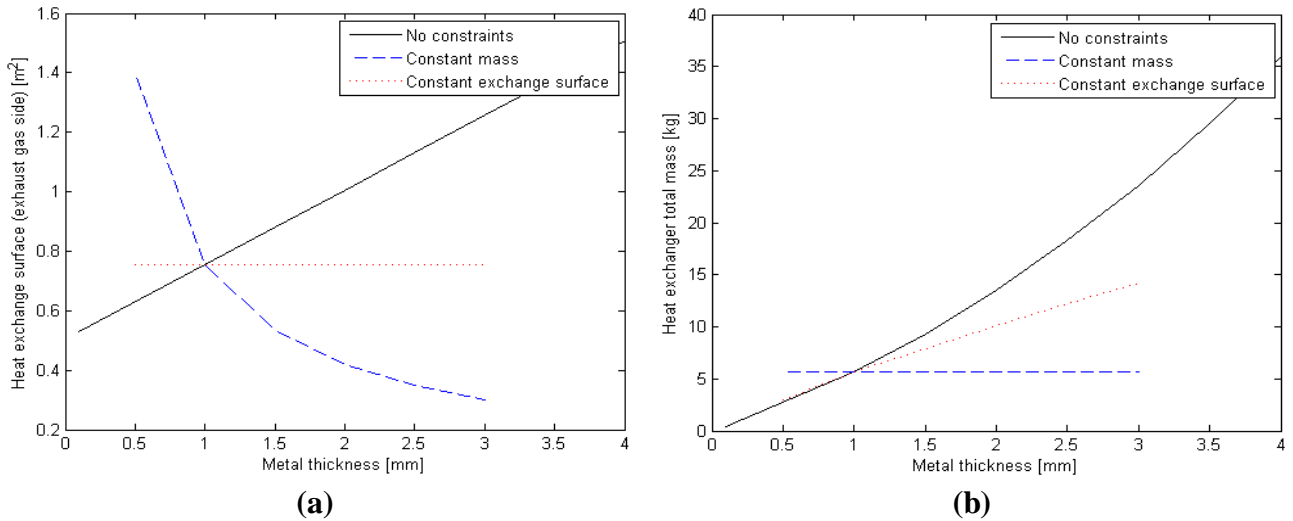


Fig. 5. Heat exchanger properties as a function of inner pipe thickness for the three investigated cases. a) inner pipe outer surface and b) total mass

The thickness of the heat exchanger was varied between different simulations in order to test its influence on the performance of the heat exchanger. Three different cases were investigated:

1. **Fixed heat exchanger length.** This corresponds to the “unconstrained” case, since in this case both the outer surface of the inner pipe and the total mass of the heat exchanger increase with the thickness of the pipe.
2. **Fixed outer surface of the inner pipe.** Since the hot side of the exchange is the limiting factor, increasing the outer surface of the inner pipe significantly benefits the overall heat exchange process. In order to isolate this effect, in this case the length of the exchanger was modified in accordance with the metal thickness to keep a constant value for the total heat exchange area on the outer side of the inner pipes.
3. **Fixed heat exchanger mass.** In several applications, weight is a constraint that should be accounted for. In this case, similarly to the previous one, the length of the heat exchanger is adapted to keep a constant heat exchanger mass.

Figures 5a and 5b show the influence of varying the wall thickness of the heat exchanger in the three different cases on the total heat exchange surface on the hot side and on the total mass of the heat exchanger, respectively. Figure 4 shows that, when no constraints are set, both surface and mass of the heat exchanger increase with increased wall thickness; on the other hand

4. Results and discussion

4.1 Heat exchange properties in the reference case

Figure 6 shows the performance of the heat exchanger in the reference case, both in steady-state and dynamic perspective. Figure 6a suggests, as expected, that the gas side of the heat exchanger represents the limiting factor for the exchange, which is confirmed by the temperature of the heat exchanger wall which closely follows that of the cold fluid. The heat exchange coefficients calculated in the model for the different parts of the heat exchanger are presented in Table 4. The convective heat exchange coefficient in the superheated part of the exchanger is particularly high as a consequence of the high speed of the fluid in this part.

Figure 6b shows how the manoeuvring phase generates a drop in outlet steam quality that continues for several minutes even after higher flow and temperature in the exhaust are restored. This results in the potential for heat recovery being limited by the potential damages arising in the expander of the system due to the formation of water droplets. Such configuration, as Figure 6b suggest, would allow the effective functioning of the WHR system only for a limited fraction of the total time spent on the field.

Table 4. Steady-state heat transfer coefficients of the reference heat exchanger.

Convective heat exchange coefficient [W/mK]	Min	Mean	Max
Gas side		96.1	
Water side (liquid)	490	849	1170
Water side (phase change)	1240	2250	2950
Water side (superheated steam)	1220	1230	1240

The observation of Figure 6b therefore suggests that despite the limited duration of the manoeuvring phase, the performance of the system would still be heavily affected by its presence for up to four minutes after the machine started its operations again at full power. In real applications this situation would be partially mitigated by the presence of a control system able to reduce the water mass flow sufficiently to ensure continuity in the operations of the expander. However, these observations suggest that a more efficient system could be designed if such variability was taken into account from a design rather than from a control perspective.

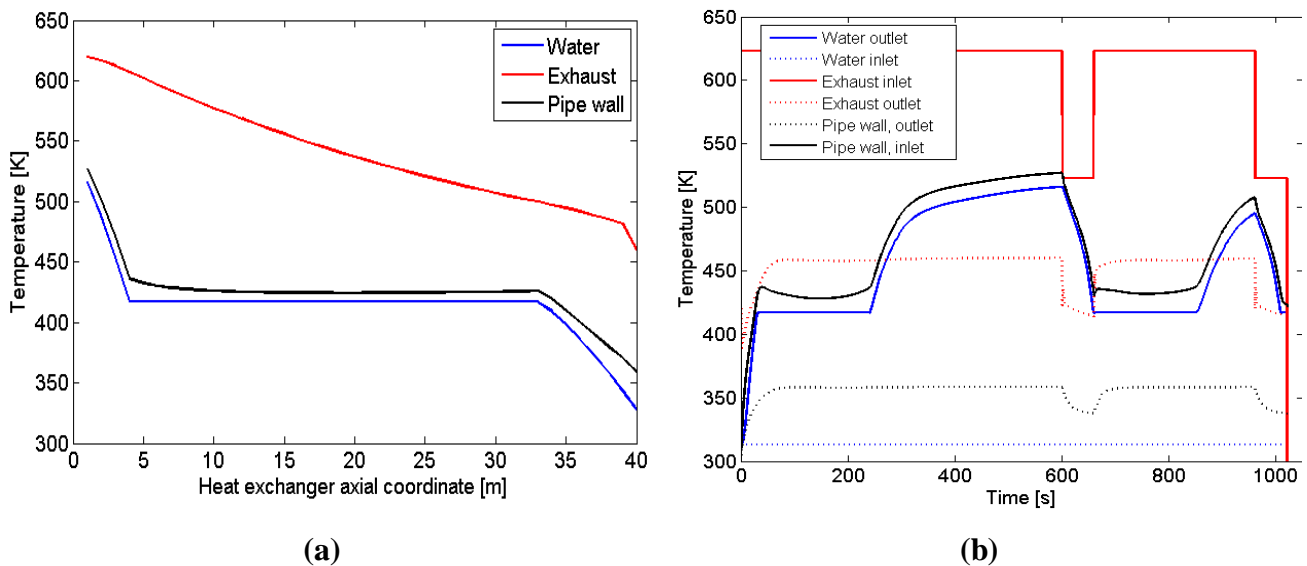


Fig. 6. Temperature profiles for the reference heat exchanger. a) Steady-state temperatures along the exchanger and b) temperature evolution over time at exchanger inlet and outlet.

4.2 Working cycle

Figure 6a shows the cumulated recoverable exergy over one manoeuvring cycle according to (11) as a function of inner wall thickness for the three investigated cases.

The observation of Figure 7a suggests that in the case where no constraints are put, the simultaneous increase in exchange surface and exchanger mass allows, for increased pipe wall thickness, a higher rate of total recovered exergy; this trend tends to reach a saturation point over 2 mm thickness, which relates to approaching the pinch limit in the heat exchanger at the beginning of the evaporation phase. From this type of analysis it does not appear clearly, however, what is the contribution of respectively increased exchange surface and increased inertia.

In the case where the mass of the exchanger is kept constant, it appears that the exchange surface is the dominant aspect to account for, and that in applications where the total mass of the exchanger

constitutes a limiting boundary condition, the designer should seek to maximise the exchange surface. In the case of a tubular heat exchanger, this translates into minimizing the wall thickness by reducing it to the minimum limit required for structural resistance.

The case at constant outer exchange surface shows the existence of a growing trend with thickness, which represents the effect of increased inertia. This effect can improve the recovered exergy over an entire cycle by 27% when pipe thickness is increased from 1 mm to 2.5 mm, shown in Figure 7a.

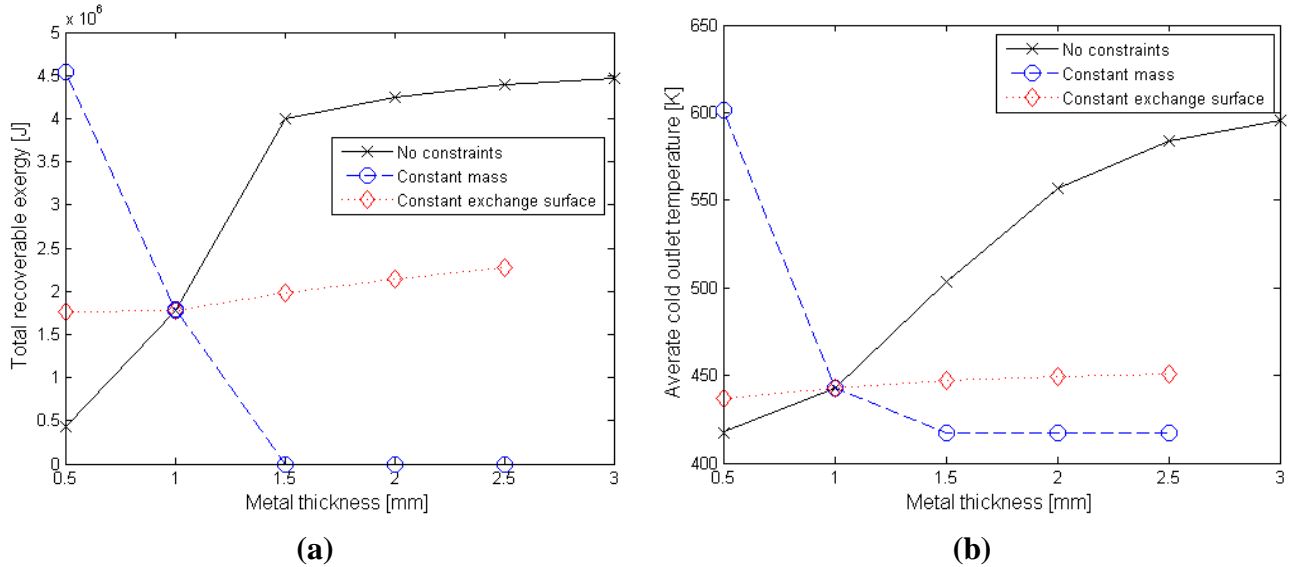


Fig. 7. Integrated values over one working-manoevring cycle for different wall thickness and for different cases. a) Recoverable exergy and b) Average temperature

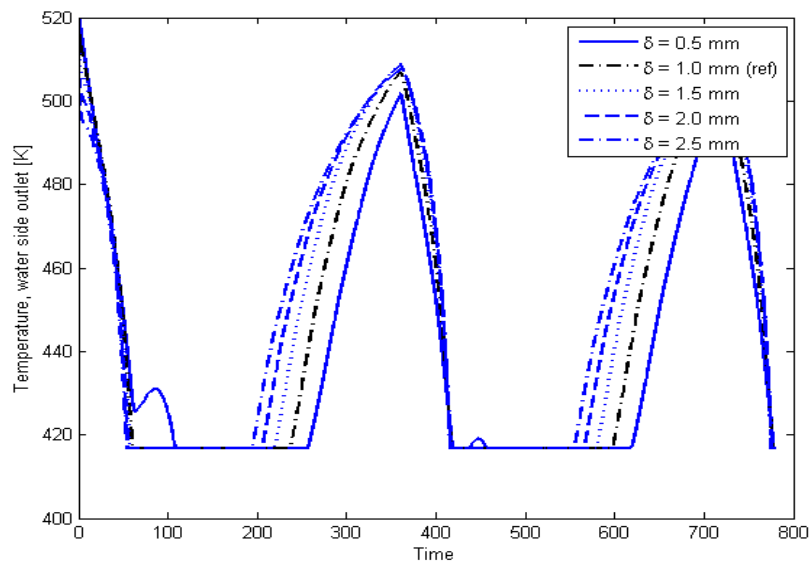


Fig. 8. Temperature evolution for two working-manoevring cycles at the cold fluid outlet. Case at fixed hot-side surface for variable wall thickness.

The evolution of cold side outlet temperature in this case (Figure 8) shows that the drop in outlet steam enthalpy during manoeuvring happens with similar speed in all cases, regardless of the thickness of the heat exchanger wall. In the cases where the wall is thicker, however, the steam at the heat exchanger outlet becomes superheated faster after the end of the manoeuvring phase.

The reason for such behaviour can be explained from the observation of Figure 9. In the case with 0.5 mm wall thickness (Figure 9a), the recovery is initially faster but later slowed down by the arrival of the colder flow from the heat exchanger inlet, which has not been heated as much because of the low inertia. In the case with wall thickness 2.5 mm (Figure 9b), instead, there is no initial

recovery, but the overall process is made faster by the fact that the drop in enthalpy in the exchanger stages close to the cold inlet is lower.

This behaviour suggests that, although the increase in heat exchanger inertia seems to bring an improvement in the transient performance of the heat exchanger in terms of recoverable exergy, in practice the largest part of the gain comes from the initial part of the heat exchanger. In particular, the part of the heat exchanger included between 0.2 and 0.3 fraction of the overall length contributes the most. The cold fluid in this part of the heat exchanger becomes sub-cooled liquid during low-load periods while evaporation takes place when the load is higher (see Figure 10); this leads to significant changes in the temperature of the heat exchanger wall during transients and consequently to higher contribution from heat storage. The part of the exchanger located between 0.3 and 0.9 of the overall heat exchanger length, where the cold fluid is in the vapour state during the whole simulation, does not change temperature and therefore does not contribute to increasing the inertia of the heat exchanger.

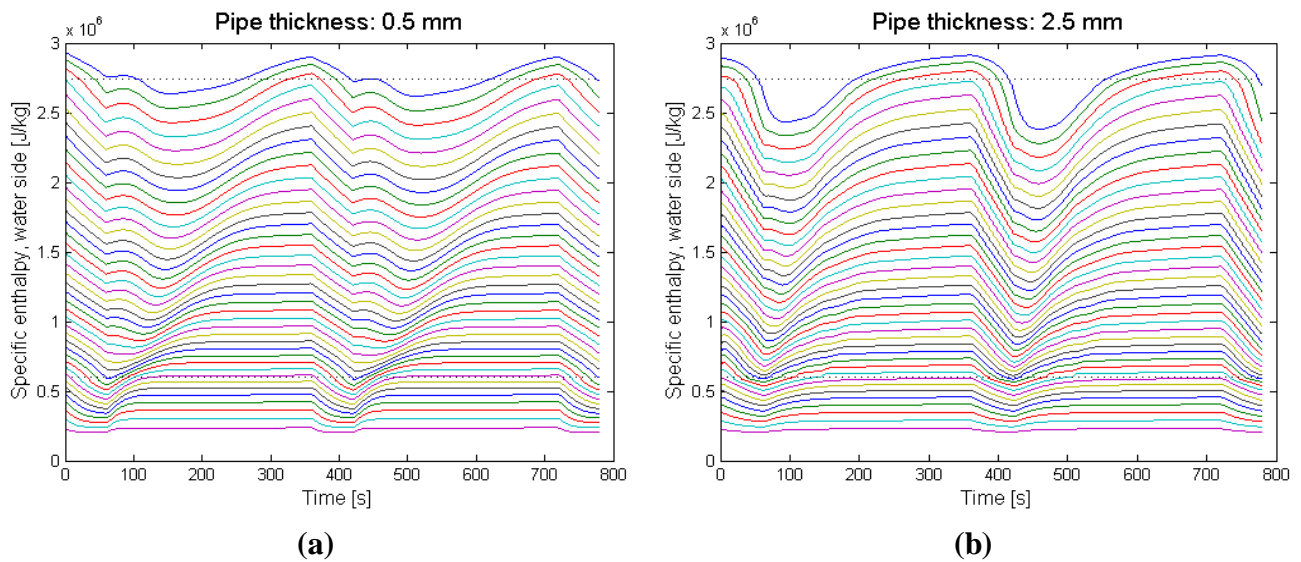


Fig. 9. Cold-side enthalpy evolution for two working-manoeuvring cycles. Different lines correspond to different locations along the heat exchanger. Case at fixed hot-side surface. a) 0.5 mm wall thickness and b) 2.5 mm wall thickness.

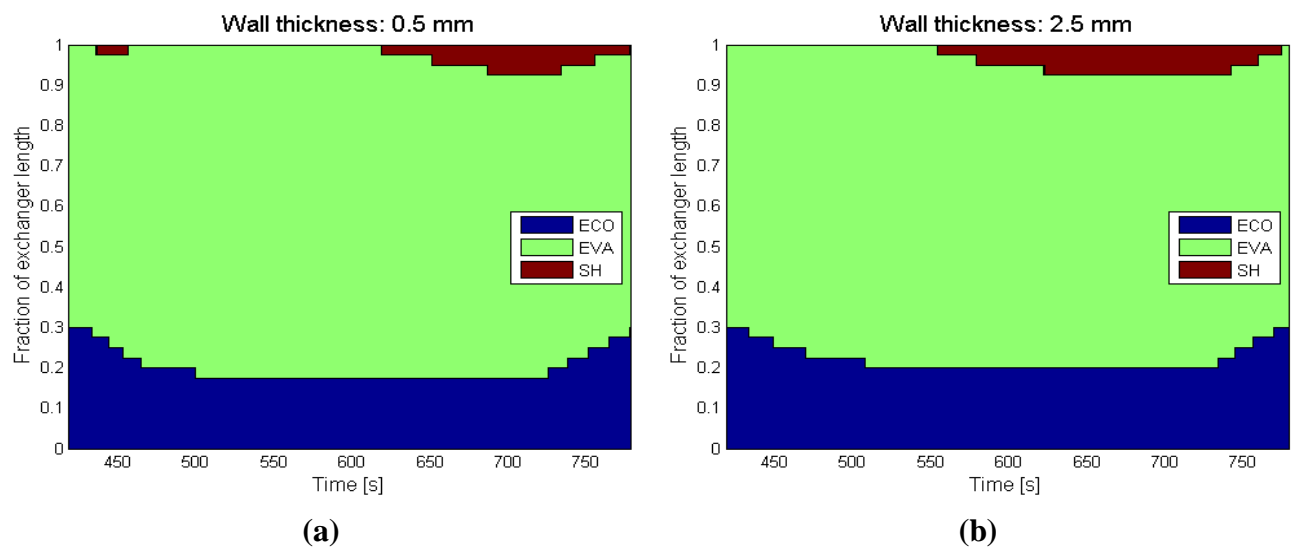


Fig. 10. Heat exchanger subdivision in subcooled, two-phase and superheated steam as a function of time for one working-manoeuvring cycle. Case at fixed hot-side surface. a) 0.5 mm wall thickness and b) 2.5 mm wall thickness

5. Conclusions

In this paper we investigated the potential for improving the available recoverable exergy from agricultural machines operations by modifying the evaporator's inertia. The cyclical behaviour of these machines, which was described in Section 2.2, justifies the effort of trying to avoid turbine cut-out during the short manoeuvring breaks which regularly occur between two high-load harvesting phases.

The results presented in this paper suggested that increasing the inertia of the heat exchanger, which in this study was modelled by an increase in the inner heat exchanger wall, can be a solution for improving the dynamic performance of the whole system. When the pipe thickness is increased from 1 mm to 2.5 mm the exergy flow at the cold outlet of the heat exchanger integrated over one harvesting-maneuver cycle increased by 27%, at constant heat exchange surface, as a consequence of the higher amount of time during which the outlet cold flow is in the superheated steam region. These results therefore suggest that heat exchanger inertia, in addition to exchange coefficient and surface, should be taken into account in the design process of waste heat recovery systems working with a cyclic, dynamic operational profile.

References

- [1] Bourhis G, Leduc P. Energy and Exergy Balances for Modern Diesel and Gasoline Engines. *Oil Gas Sci Technol D Ifp Energies Nouv* 2010;65:39–46.
- [2] Armstead JR, Miers SA, Asme. Review of waste heat recovery mechanisms for internal combustion engines. New York: Amer Soc Mechanical Engineers; 2010.
- [3] Sprouse Charles DC. Review of organic Rankine cycles for internal combustion engine exhaust waste heat recovery. *Appl Therm Eng* 2013;51:711–22.
- [4] Espinosa Tilman, Loic , Lemort, Vincent, Quoilin, Sylvain, Lombard, Benoit N. Rankine cycle for waste heat recovery on commercial trucks: approach, constraints and modelling. *Diesel Int Conf Exhib* 2010.
- [5] Yang Min-Hsiung YR-H. Analyzing the optimization of an organic Rankine cycle system for recovering waste heat from a large marine engine containing a cooling water system. *Energy Convers Manag* 2014;88:999–1010.
- [6] Macián V. Dolz V. ,Sánchez J. SJR. Methodology to design a bottoming Rankine cycle, as a waste energy recovering system in vehicles. Study in a HDD engine. *Appl Energy* 2013;104.
- [7] Wang Tianyou Peng Zhijun, Shu Gequn ZY. A review of researches on thermal exhaust heat recovery with Rankine cycle. *Renew Sustain Energy Rev* 2011;15.
- [8] Shokati N, Mohammadkhani F, Farrokhi N, Ranjbar F. Thermodynamic and heat transfer analysis of heat recovery from engine test cell by Organic Rankine Cycle. *Heat Mass Transf* 2014;50:1661–71.
- [9] Larsen U, Pierobon L, Haglind F, Gabriellii C. Design and optimisation of organic Rankine cycles for waste heat recovery in marine applications using the principles of natural selection. *Energy* 2013;55:803–12.
- [10] Livanos G a., Theotokatos G, Pagonis D-N. Techno-economic investigation of alternative propulsion plants for Ferries and RoRo ships. *Energy Convers Manag* 2014;79:640–51.
- [11] Kalikatzarakis M, Frangopoulos CA. Multi-criteria selection and thermo-economic optimization of Organic Rankine Cycle system for a marine application. *Proceedings 27th Int. Conf. Effic. Cost, Optim. Simulation, Environ. Impact Energy Syst.*, Turku, Finland: 2014.
- [12] Dimopoulos GG, Georgopoulou CA, Kakalis NMP. Modelling and optimization of an integrated marine combined cycle system. *Proc. Int. Conf. Effic. Cost, Optim. Simul. Environ. Impact Energy Syst.*, Novi Sad: 2011.

- [13] Shu G, Liang Y, Wei H, Tian H, Zhao J, Liu L. A review of waste heat recovery on two-stroke IC engine aboard ships. *Renew Sustain Energy Rev* 2013;19:385–401.
- [14] Burel F, Taccani R, Zuliani N. Improving sustainability of maritime transport through utilization of Liquefied Natural Gas (LNG) for propulsion. *Energy* 2013;57:412–20.
- [15] Choi BC, Kim YM. Thermodynamic analysis of a dual loop heat recovery system with trilateral cycle applied to exhaust gases of internal combustion engine for propulsion of the 6800 TEU container ship. *Energy* 2013;58:404–16.
- [16] Feru E, Kupper F, Rojer C, Seykens X, Scappin F, Willems F, et al. Experimental Validation of a Dynamic Waste Heat Recovery System Model for Control Purposes. *SAE Int* 2013.
- [17] Quoilin S, Aumann R, Grill A, Schuster A, Lemort V, Spliethoff H. Dynamic modeling and optimal control strategy of waste heat recovery Organic Rankine Cycles. *Appl Energy* 2011;88:2183–90.
- [18] Lee YR, Kuo CR, Liu CH, Fu BR, Hsieh JC, Wang CC. Dynamic Response of a 50 kW Organic Rankine Cycle System in Association with Evaporators. *Energies* 2014;7:2436–48.
- [19] Lacour S, Descloux S, Baldi F, Podvin P. Waste heat recovery on tractor engine: exergy analysis of exhaust in transient conditions. In: Pitesti U of, editor. *Automot. Ser. Year XVII*, vol. 21, Pitesti: 2011, p. 145–52.
- [20] Nielsen RF, Haglind F, Larsen U. Design and modeling of an advanced marine machinery system including waste heat recovery and removal of sulphur oxides. *Energy Convers Manag* 2014;85.
- [21] Feru E, Willems F, Jager B De, Steinbuch M. Modeling and Control of a Parallel Waste Heat Recovery System for Euro-VI Heavy-Duty Diesel Engines. *Energy Procedia - Proc. Int. Conf. Appl. Energy, Taipei, Taiwan: 2014*, p. 1–20.
- [22] Hadidi M, Guellal M, Lachi M, Padet J. Loi de reponse d'un echangeur thermique soumis a des echelons de temperature aux entrees. *Int Commun Heat Mass Transf* 1995;22:145–54.
- [23] Henrion M, Feidt M. Comportement en regime transitoire de divers types d'echangeurs de chaleur ; Modelisation et consequences. *Int Commun Heat Mass Transf* 1991;18:731–40.
- [24] Morales-Ruiz S, Rigola J, Rodriguez I, Oliva A. Numerical resolution of the liquid-vapour two-phase flow by means of the two-fluid model and a pressure based method. *Int J Multiph Flow* 2012;43:118–30.
- [25] Feru E, de Jager B, Willems F, Steinbuch M. Two-phase plate-fin heat exchanger modeling for waste heat recovery systems in diesel engines. *Appl Energy* 2014;133:183–96.
- [26] Lacour S, Burgun C, Perilhon C, Descombes G, Doyen V. A model to assess tractor operational efficiency from bench test data. *J Terramechanics* 2014;54:1–18.
- [27] Quoilin S. Sustainable energy conversion through the use of organic Rankine cycles for waste heat recovery and solar applications. University of Liege, 2011.
- [28] Von Böckh P, Wetzel T. Heat transfer: basics and practice. Berlin Heidelberg, Germany: Springer; 2011.
- [29] Quoilin S, Bell I, Desideri A, Dewallef P, Lemort V. Methods to Increase the Robustness of Finite-Volume Flow Models in Thermodynamic Systems. *Energies* 2014;7:1621–40.
- [30] Cengel YA, Turner RH. Fundamentals of thermal-fluid sciences. 2nd editio. New York: McGraw-Hill; 2005.